Journal of Ovonic Research Vol. 12, No. 2, March - April 2016, p. 75 - 80

EFFECT OF CALCINATION TEMPERATURE ON THE SIZE AND OPTICAL PROPERTIES OF SYNTHESIZED ZnO NANOPARTICLES

E. G. MORNANI[a], P. MOSAYEBIAN[a], D. DORRANIAN[a], K. BEHZAD[b*]
[a]*Laser Lab., Plasma Physics Research Center, Science and Research Branch, Islamic Azad University, Tehran, Iran*
[b]*Department of Physics, Shahr-e-Qods Branch, Islamic Azad University, Tehran , Iran*

ZnO nanoparticles (NPs) were synthesized through a very facile chemical reduction method in ethylene glycol solvent at six different calcination temperatures. Effect of variation in calcination temperature was studied using X-ray diffraction (XRD), transmission electron microscopy (TEM), Fourier-transform infrared (FTIR), and UV-Vis spectroscopy. In this work, the effect of calcination temperature on the particle size and optical properties of ZnO nanoparticles was also studied. For structural characterization, ZnO NPs were characterized by XRD and TEM. The impurity contents were characterized by FTIR spectroscopy. Synthesized ZnO nanoparticles exhibited a hexagonal structure with sizes from 46 to 66 nm. The studies revealed a blue shift in UV-Vis spectra with rising the calcination temperature. The investigations also revealed that bandgap of ZnO NPs is wider than that of bulk ZnO where rising the temperature increases the bandgap up to 4.45 eV.

(Received February 3, 2016; Accepted March 30, 2016)

Keywords: ZnO nanoparticle, Synthesis, Calcination, XRD, TEM, FTIR, UV-Vis Spectroscopy.

1. Introduction

Semiconductor nanomaterial demonstrates unique properties which are not shown by their bulk materials. These properties in nanoscale dimension are size dependent and start to appear when the size of particles is about Bohr diameter for exciton [1]. Among the semiconductor nanoparticles (NPs), zinc Oxide (ZnO), with binding energy of 60 meV and a wide electronic band gap of 3.3 eV, has drawn a great deal of attention to itself due to its wide range of applications such as varistors [2, 3], UV absorber [4], antibacterial [5, 6], light emitters [7, 8], dye degradation [9, 10], solar cells [11-13], gas sensors [14, 15], photoluminescence materials [16, 17], and transparent conductors [18]. Different synthesis methods have been introduced for the preparation of ZnO NPs [19-22] and among them, the chemical reduction method is considered as one of the most advantageous route due to being low cost method and needless of any surfactant. However, in the chemical method, size control is an obstacle since the addition of reducing agent results in a fast nucleation and subsequently aggregation of particles. Moreover, fast nucleation eventuates in a heterogeneous crystal phase. A post processing such as thermal treatment can resolve these problems. Thermal treatment, for example calcination, would eliminate impurities and the second chemical phase, used as the capping agent, resulting in a pure product. Besides, calcination effectively modifies the crystal phase resulting a homogenous one. Therefore, the combination of these two methods, chemical and thermal, makes it possible to exploit the advantageous of two methods and producing nanoparticles with finer size and better crystal phase. In this work, we report a facile route to synthesize ZnO NPs. ZnO NPs are first synthesized by a chemical method. The products subsequently calcined at different temperatures. The structural and optical properties of NPs at various calcination temperatures were studied by different characterization methods.

*Corresponding author: kasra.behzad@gmail.com

2. Materials and Method

Zinc nitrate hexahydrate ($Zn(NO_3)_2 \cdot 6H2O$), as the precursor, ethylene glycol ($C_2H_6O_2$), as the capping agent, and hydrazine (N_2H_4), as the reducing agent, were used to synthesise the ZnO NPs. All the materials were of analytical purity. 1N solution of zinc nitrate was prepared by dissolving the appropriate amount of salt in ethylene glycol. For preparing the 2N hydrazine, the appropriate amount of hydrazine was dissolved in distilled water. Solutions of $Zn(NO_3)_2$ and N_2H_4 were simultaneously mixed under stirring for one hour. The solution was filtered and then the residual solid were dried at 80 ^oC in an oven for five hours. To obtain ZnO NPs, The final product was calcined at different temperatures of 400, 450, 500, 550, 600, and 650 °C in air for 8 hours.

ZnO-NP samples at six different temperatures and the powder sample before calcination were characterized using X-ray diffraction (XRD), Fourier transform infrared spectroscopy (FTIR), transmission electron microscopy (TEM), and UV-Vis spectroscopy. Phase evolutions and structure of ZnO-NPs were studied by XRD (Stoe, Stadi MP Cu Kα 1, λ=1.54 A^0) and FTIR (Perkin Elmer, Spectrum 100). Optical absorption spectra were recorded on a Shimadzu UV-1800.

3. Results and discussion

Fig. *1* shows a typical FTIR absorption spectrum of ZnO NP calcined at 650 ^oC. The peak at 580 cm^{-1} is a characteristic absorption of Zn–O bond. The weak and broad absorption peak at the wavenumber of 3440 cm^{-1} is attributed to the characteristic absorption of hydroxyls. For all samples in the study, one strong absorption band was observed at 580 cm^{-1} that corresponds to ZnO. Same IR signatures have been reported for ZnO NPs in many literatures [23-25].

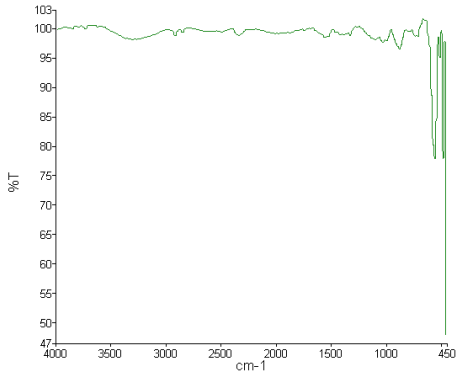

Fig. 1. Typical FTIR spectrum of ZnO NP was calcinated at 650 ^oC.

ZnO crystals as a II-VI compound semiconductor are found to grow in two forms, hexagonal wurtzite, cubic zinc blende, and rarely observed cubic. Fig 2 shows the XRD patterns of samples before and after calcination at different calcination temperatures.

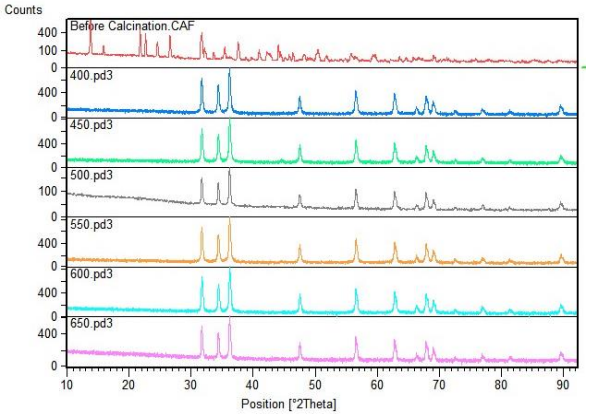

Fig 2. X-ray diffraction patterns of the samples before and after calcination at different temperatures.

The XRD pattern for samples before and after calcination, suggests the effect of calcination on samples. This effect indeed resulted in formation of hexagonal phase crystals. The X-ray diffraction peaks for (100), (002), (101), (102) (110), (103) and (112) planes confirm the formation of hexagonal wurtzite structure of ZnO. The mentioned values for the ZnO are assigned to JCPDS card no. 01-080-0075. The main peaks of ZnO hexagonal wurtzite are shown in all patterns. Data analysis of before and after calcination samples, reveal that hexagonal wurtzite phase of ZnO were formed by calcination at different temperatures.

Debye Scherrer's formula was used to estimate the crystallite size,

$$D = \frac{0.94\lambda}{\beta \cos\theta} \tag{1}$$

where, D is the crystallite size, λ=1.54Å is the X-ray source wavelength, β is the FWHM of a peak, and θ is the peak position. The extracted average size are in the range of 46-66nm. Fig. *3* shows the variation of NPs size as a function of calcination temperature. It reveals that increasing the calcination temperature results in smaller size of NPs. Under the mentioned conditions, the calcined sample at 650 ^{o}C was demonstrated the smallest size.

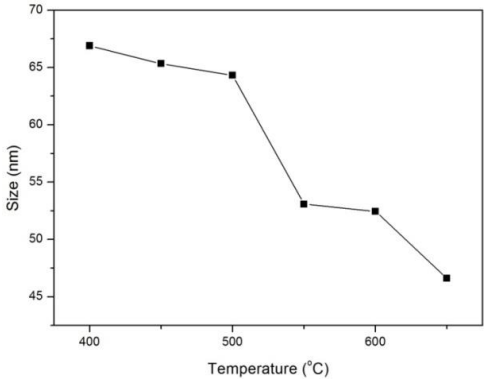

Fig. 3. ZnO NP size as function of temperature.

Fig. *4* shows a typical TEM image of ZnO NPs that was calcined at 650 ^{o}C. Extracted sizes from TEM images are in the good agreement with the calculated size by XRD.

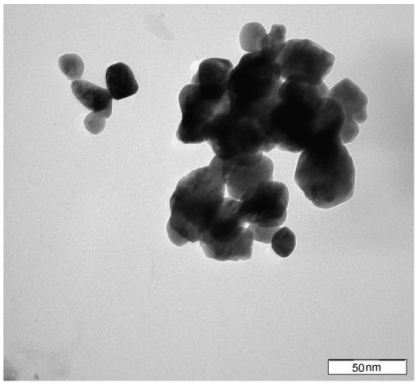

Fig. 4. Typical TEM image of ZnO NPs.

The optical properties and electronic band gap energies of ZnO NPs were analyzed using UV–Vis spectroscopy. The room temperature UV-Vis absorption spectra of the dispersed ZnO NPs in ethylene glycol are represented in Fig. *5*.

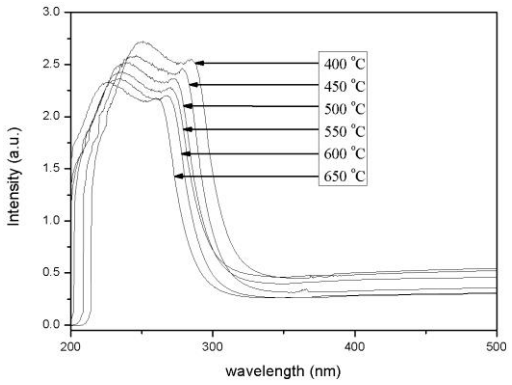

Fig. 5. UV-Vis spectra of diluted ZnO NPs in ethylene glycol.

These spectra shows absorption bands between 200-500 nm and indicates a blue-shift compared to the bulk ZnO (~3.38 eV=367 nm)[25]. The blue-shift occurs due to the quantum confinement effect in nanoscale materials. Fig. *5* reveals that absorption peak is blue-shifted by increasing the calcination temperature due to the size reduction. Optical band gaps were calculated from Tauc relation and extrapolation procedure. Fig 6 illustrates a typical extrapolation of the absorption spectrum related to the sample with calcination temperature of 500 ^{o}C.

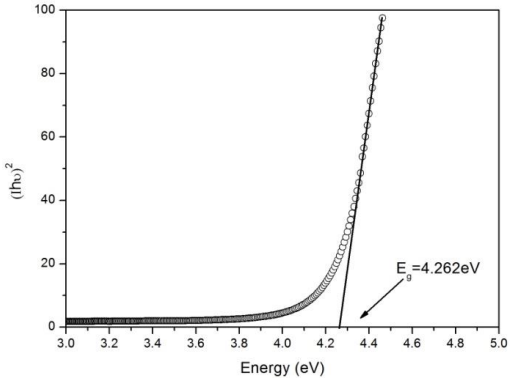

Fig 6. (Ihv)^2 versus energy for the sample with calcination temperature of 500 ^{o}C.

The optical absorption was plotted versus the incident photon energy, and the value of the band gap energy was determined by extrapolating the linear part of the graph. Each graph was extrapolated for $(\alpha h\nu)^2 = 0$ to find the band gap [26, 27]. The calculated band gaps of the samples are plotted in Fig. *7*. This result indicates that the band gap energy can be tuned by varying the calcination temperature for different applications. As shown in Fig. *7*, the band gap was tuned from 4.08 to 4.45 eV by raising the temperature from 400 to 650^{o}C.

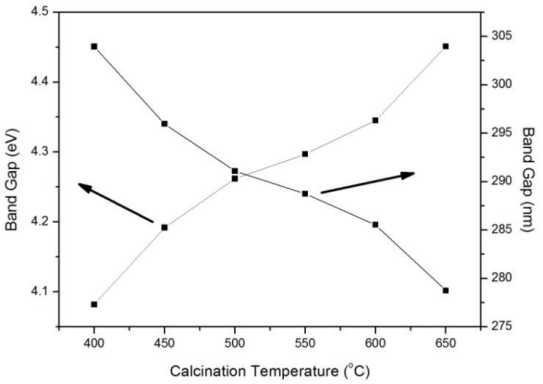

Fig. 7. Band gap vs. calcination temperature for all samples.

Fig. *8* shows variation of band gap energy as function of ZnO NP size [28].

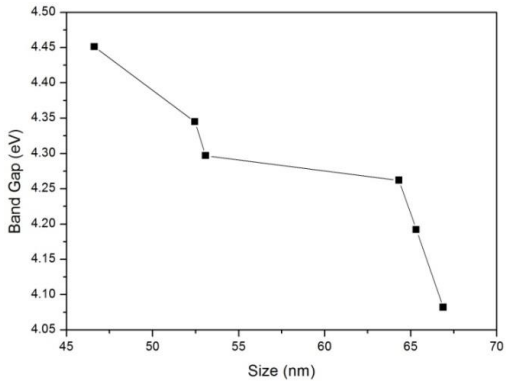

Fig. 8. Band gap vs. particle size for all samples.

4. Conclusions

ZnO NPs were obtained using chemical reduction method and the size of particles was about 46-66 nm. Structural characterizations, using XRD, FTIR, and TEM, revealed that pure ZnO particles in the nano scale were prepared. The NP size became smaller by rising the calcination temperature from 400 to 650 ^{o}C. Temperature increment, in the mentioned range, reduced the particle size from 66 to 46 nm. UV-Visible spectroscopy indicated that the UV-Vis absorption characteristics can be tuned by varying the calcination temperature. Blue shift in UV-Visible spectra occurs by rising the calcination temperature. The origin of the blue shift has been attributed to decreasing the size effect. The absorption intensity decreased with reduction in size of ZnO NPs. Bandgap evaluation of the ZnO NPs revealed that increasing the calcination temperature result in the wider bandgap from 4.08 to 4.45 eV. Band gap expansion was caused by the quantum confinement effect due to the reduction in size of NPs.

References

[1] M.Bangal, S. Ashtaputre, S. Marathe, A. Ethiraj, N. Hebalkar, S. W. Gosavi, J. UrbanS. K. Kulkarni,Hyperfine Interactions **160**, 81 (2005).

[2] L.-H.,Cheng, L.-Y. Zheng, L. Meng, G.-R. Li, Y. Gu, F.-P. Zhang, R.-Q. Chu Z.-J. Xu, Ceramics International **38**, S457 (2012).

[3] R. K.,Sendi, S. Mahmud, A. MunshiA. Seeni. In vitro cytotoxicity tests of ZnO-Bi_2O_3-Mn_2O_3-based varistor fabricated from ZnO micro and nanoparticle powders on L929 mouse cells. in 3rd International Conference on Fundamental and Applied Sciences (ICFAS 2014): Innovative Research in Applied Sciences for a Sustainable Future. 2014: AIP Publishing.

[4] F. Grüneberger, T. Künniger, A. Huch, T. ZimmermannM. Arnold,Progress in Organic Coatings **87**, 112 (2015).

[5] Y.,Qian, J. Yao, M. Russel, K. ChenX. Wang,Environmental toxicology and pharmacology **39**, 736 (2015).

[6] D.,Thomas, J. Abraham, C. V. Sunil, S. AugustineT. Dennis Thomas,Indo American Journal of Pharmaceutical Research **4**, 1612 (2014).

[7] S.F. Pearton, Ren,Current Opinion in Chemical Engineering **3**, 51 (2014).

[8] P.-N.,Ni, C.-X. Shan, B.-H. LiD.-Z. Shen,Applied Physics Letters **104**, 4 (2014).

[9] Dutta, R. K., B. P. NenavathuS. Talukdar,Colloids and Surfaces B: Biointerfaces **114**, 218 (2014).

[10] Y., Abdollahi, A. Zakaria, A. H. Abdullah, H. R. F. Masoumi, H. Jahangirian, K. Shameli, M. Rezayi, S. BanerjeeT. Abdollahi,Chem Cent J **6**, 88 (2012).

[11] D.-Y.,Son, J.-H. Im, H.-S. KimN.-G. Park,The Journal of Physical Chemistry C **118**, 16567 (2014).

[12] M.,Hosni, T. Pauporté, S. FarhatN. Jouini. Effects of annealing temperature and thickness of nanoparticle ZnO aggregate layers on dye-sensitized solar cell performances. in SPIE OPTO. 2015: International Society for Optics and Photonics.

[13] M., Saleem, L. Fang, M. Ashfaq Ahmad, R. Raza, F. Wu, W. J. Li, C. L. Xu, L. Hu S. J. Xue,Nano **09**, 1450061 (2014).

[14] J.,Guo, J. Zhang, M. Zhu, D. Ju, H. XuB. Cao,Sensors and Actuators B: Chemical **199**, 339 (2014).

[15] O. A.,Fouad, G. GlaspellM. S. El-Shall,Nano **05**, 185 (2010).

[16] M.,Koleva, A. O. Dikovska, N. Nedyalkov, P. AtanasovI. Bliznakova,Applied Surface Science **258**, 9181 (2012).

[17] J. G.,Simmons Jr, J. V. Foreman, J. LiuH. O. Everitt,Applied Physics Letters **103**, 201110 (2013).

[18] El Yamny, S.M. A. Rafea,Journal of Modern Physics **3**, 1060 (2012).

[19] S. C.Das, , B. Tudu, N. Bhattacharyya, R. BandyopadhyayP. Pramanik, Doped ZnO Nanostructured Sensor in Electronic Nose for Detection of Ammonia, Hydrogen and Liquefied Petroleum Gas, in Advanced Nanomaterials and Nanotechnology. 2013, Springer. p. 475-484.

[20] P., Swain, S. Nayak, A. Sasmal, T. Behera, S. Barik, S. Swain, S. Mishra, A. Sen, J. Das P. Jayasankar,World Journal of Microbiology and Biotechnology **30**, 2491 (2014).

[21] W.Xia, , C. Mei, X. Zeng, G. Fan, J. Lu, X. MengX. Shen,ACS applied materials & interfaces **7**, 11824 (2015).

[22] S. Brahma, S. A. Shivashankar,Current Nanoscience **9**, 346 (2013).

[23] A.,Šarić, S. MusićM. Ivanda,Journal of Molecular Structure **993**, 219 (2011).

[24] B., Cheng, Y. Xiao, G. WuL. Zhang,Applied physics letters **84**, 416 (2004).

[25] K.,Ghule, A. V. Ghule, B.-J. ChenY.-C. Ling,Green Chemistry **8**, 1034 (2006).

[26] N.,Soltani, A. Dehzangi, E. Saion, B. Y. Majlis, M. R. Zare, A. Kharazmi M. Navasery,Chalcogenide Letters **10**, 27 (2013).

[27] A., Kharazmi, N. Faraji, R. M. Hussin, E. Saion, W. M. M. YunusK. Behzad,Beilstein journal of nanotechnology **6**, 529 (2015).

[28] Y.,Masuda, M. Yamagishi, W. S. SeoK. Koumoto,Crystal Growth and Design **8**, 1503 (2008).